J4J.3 ANALYSIS OF VERTICAL MOTIONS IN FINE SCALE PRECIPITATION BANDS IN WINTER CYCLONES USING WIND PROFILER DOPPLER SPECTRA

Marcia R. Estrem[1], Robert M. Rauber[1], Kevin R. Knupp[2], Brian F. Jewett[1], Justin T. Walters[2], and Dustin Phillips[2]
[1]University of Illinois at Urbana-Champaign, Urbana, IL
[2]University of Alabama in Huntsville, Huntsville, AL

1. INTRODUCTION

Mesoscale precipitation bands often develop in the north and northwest quadrants of extratropical cyclones (Novak et al. 2004) and can produce locally large amounts of snow, sleet and freezing rain in areas adjacent to little or no precipitation. The fine-scale characteristics of winter precipitation make it difficult to fully understand and forecast the location, duration, type and amount of precipitation at the onset of winter storms. Knowing the magnitude of vertical air motions within bands of winter cyclones aids in determining the formation mechanisms of the bands and could eventually improve techniques by which they are forecast.

One uncertainty concerning mesoscale bands is the magnitude of the vertical motions occurring within them; are they characteristic of synoptic scale ascent (of the order of cm s^{-1}) or of weak convection (of the order of m s^{-1})? Theoretical predictions for moist symmetric instability (MSI) under inviscid conditions predict vertical velocities of the order of 1 m s^{-1} (Emanuel 1983, see also Bluestein 1993, p. 556-559). Maximum vertical motions for MSI when turbulent mixing is considered is of the order of 10 cm s^{-1} (e.g., Bennetts and Hoskins 1979, P. 954-957; Knight and Hobbs 1988, their Figs. 8, 11; Xu 1992, P. 637; Persson and Warner 1995, their Fig. 13; Innocentini et al. 1992, P.1099; Zhang and Cho 1995, their Fig. 3).

A greater understanding of the magnitude of vertical motions in precipitation bands in cool season cyclones comes primarily from measurements of rainbands made in the northwest United States and reported in a series of papers by Hobbs et al. (1980); Herzegh and Hobbs (1980); Houze et al. (1981); Herzegh and Hobbs (1981); Wang et al. (1983); Wang and Hobbs (1983); Locatelli and Hobbs (1987); Hertzman and Hobbs (1988) and Hertzman et al. (1988). The range of vertical velocities found was between 0.6 and 3.0 m s^{-1}. Measurements of vertical motions in banded precipitation outside the Pacific Northwest are rare, with values ranging from 0.15 to 1.5 m s^{-1} in East coast cyclones and a Midwest ice storm (Sanders and Bosart 1985a,b; Rauber et al. 1994; Wolfsberg et al. 1986; Sienkiewicz et al. 1989; Geerts and Hobbs 1991).

A small field project, Profiling of Winter Storms (PIOWS), was developed to study the structure of fine-scale winter precipitation bands. The placement of a mobile wind profiler in the path of several winter storms in the central U.S. in January and February of 2004 allowed for high-resolution measurements of the vertical structure of bands within three winter precipitation events.

The data revealed bands up to 6 km deep, 10 – 50 km wide, and spaced about 5 – 20 km apart. Measurements of vertical air motion within these bands were retrieved from the Doppler spectra using the "Lower-Bound Method" (Probert-Jones and Harper 1961; Atlas et al. 1973, P. 28), adapted to account for the effects of spectral broadening caused by the horizontal wind, wind shear, and turbulence. The purpose of this paper is to present these measurements. Section 2 provides a summary of the instrumentation, data and methodology to obtain the vertical motion within the bands. Details of the three intensive operation periods (IOPs) are given in Section 3, followed by the results in Section 4. A discussion of the results and conclusions are in Section 5.

2. METHODOLOGY

The goal of this project was to use the MIPS Doppler spectra from a 915-MHz Doppler wind profiler to derive vertical air motions, *w*, within the bands of winter cyclones. Spectra were analyzed every half-kilometer at each time interval through several bands in each cyclone.

Variations in particle radial velocity as particles approach or retreat from the profiler contribute to the spread of the power spectrum. Variations in particle radial velocity are associated with variations in particle terminal fall velocity, the mean horizontal wind due to the finite beam width, vertical wind shear within a range gate, and variations in vertical air motion due to turbulence (Battan and Theiss 1966; Atlas et al. 1973; Battan 1973; Rogers et al. 1996).

2.1. *Estimating vertical air motion from power spectra*

The process of retrieving the vertical air velocity used in this paper, the Lower-Bound Method, was first developed by Probert-Jones and Harper (1961) and adapted by Battan and Theiss (1966). It was later used

[1]*Corresponding author address:*
Robert M. Rauber, Dept. of Atmospheric Sciences,
Univ. of Illinois at Urbana-Champaign,
Urbana, IL 61801
e-mail: r-rauber@uiuc.edu

by Battan (1973) and adjusted in this study to account for the effects of spectral broadening due to the mean horizontal wind, wind shear and turbulence (Donaldson and Wexler 1969; Atlas 1964). Atlas et al. (1973) note that "the lower-bound method should work quite well in the case of snow."

The Lower-Bound Method attempts to determine the radial velocity of the smallest detectable particles within the radar beam. The smallest particles have the lowest terminal velocity and therefore can be assumed to most closely follow the air motion. The smallest detectable particles are represented in the Doppler power spectra at the rightmost point at least two standard deviations above the noise level (dot in Fig. 1). The first step in the Lower-Bound Method is to determine the radial velocity at this point (*V*).

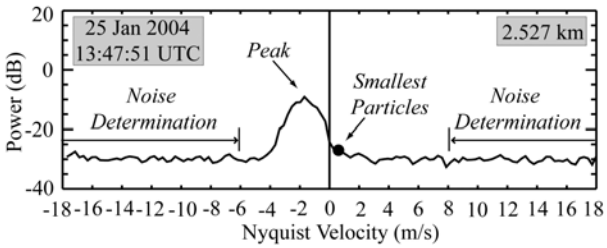

Figure 1. Doppler power spectrum taken from 915-MHz Doppler wind profiler.

The noise level was determined by calculating the mean of the power in the velocity intervals of +8 to +18.16 m s^{-1} (the positive Nyquist velocity) and -6 to -18.16 m s^{-1} (within the areas bounded by arrows in Fig. 1). The maximum velocity (*V*) with a power value at least two standard deviations above the noise level was then determined using the following algorithm.

The point to the right of the peak of the Doppler spectrum that fell below a power value two standard deviations above the mean noise power level was identified. The velocity at the point to the immediate left of this first noise point was assigned as *V* and used in subsequent calculations to estimate the vertical air velocity using the lower-bound method, with one exception. The MIPS profiler algorithm for acquiring data included ground clutter suppression which effectively reduced the power at 0 m s^{-1} to a value below the mean noise in the power spectrum. If the first point to the right of the peak of the Doppler spectrum was at 0 m s^{-1}, the next point to the right was also examined. If the power at this point was greater than two standard deviations above the mean noise power level, then the noise point at 0 m s^{-1} was ignored in the determination of *V*.

Although the particles contributing to the power at velocity *V* are the smallest and most closely follow the air motion, they have a non-zero terminal velocity. To estimate *w*, their terminal velocity must be taken into account. There were no aircraft measurements of particle size distributions or habits collected within the precipitation bands during this study. To estimate particle terminal velocities, measurements taken from similar bands in a winter storm reported by Passarelli (1978) were used.

Particle size spectra at four flight altitudes sampled by Passarelli during a period of moderate to heavy snowfall over Champaign, IL on 26 November 1975 were derived from data collected with an optical array precipitation spectrometer. Passarelli, using a precipitation particle camera, primarily observed aggregates of side plane type crystals at the 4.35 km and 3.75 km altitudes, and dendritic type aggregates at the 3.15 km and 2.55 km altitudes. Terminal velocity-diameter relationships developed by Locatelli & Hobbs (1974) for side plane aggregates

$$V_{0_s} = 0.82D^{0.12} \tag{1}$$

and dendritic type aggregates

$$V_{0_d} = 0.8D^{0.16} \tag{2}$$

with the density correction factor from Foote and DuToit (1969)

$$V_T(D) = V_0(D)\left[\frac{\rho_0}{\rho}\right]^{0.4} \tag{3}$$

were applied to estimate the fall velocities of the ice particles observed by Passarelli.

The reflectivity-weighted contribution of particles to the terminal fall velocity

$$V_t(D) = \frac{n(D)D^6 V_T(D)\Delta D}{\sum n(D)D^6 \Delta D} \tag{4}$$

was then determined for each of the size spectra in Passarelli (1978). The smallest-sized ice particles that had a non-negligible contribution to the power in the Doppler spectrum ranged in diameter from 0.5 to 0.9 cm and the smallest detectable particles ($V_{T_{\min}}$) at the four altitudes had terminal velocities between 0.83 and 0.87 m s^{-1}. We chose a single, conservative value of 0.8 m s^{-1} to estimate the terminal velocities of the smallest particles detected by the profiler at all altitudes between the top of the bands and one kilometer above the melting level, since the range of snowflake fallspeeds is narrow (Atlas et al. 1973).

Because of the 9° beam width in the vertical beam of the profiler, there is a contribution to the radial velocity by the mean horizontal wind which contributes to broadening of the power spectrum. The greatest contribution to the radial velocity comes from particles near the edge of the beam. Further broadening is induced if vertical wind shear is present, since the radial velocity of the particles near the edge of the beam will vary across a range gate. Finally, turbulence induces variations in the vertical motion field, which further broadens the power spectrum.

To account for each of these factors, we took the following approach. The wind speed ($\bar{u}$) and vertical wind shear (u') at each range gate were determined through temporal interpolation of three soundings taken at Lincoln, IL (KILX) during corresponding times for IOP1. For IOP2, these parameters were determined through temporal and spatial interpolation of soundings from Nashville, TN (KBNA), Peachtree City, GA (KFFC)

and Birmingham, AL (KBMX). The winds for IOP3 were determined from the same sounding locations, but using different times. We had no measurements of the turbulent intensity within the clouds. To estimate the turbulence we assumed that the vertical wind fluctuations scaled with the vertical wind shear (Rogers et al. 1996), since vertical wind shear will induce tumbling motions in air.

With this assumption, we can write the maximum radial velocity at the edge of the profiler beam associated with smallest detectable particles (V) as

$$V = \left(\bar{u} + u'\right)\sin\theta + \left(w + w' + V_{T_{\min}}\right)\cos\theta \qquad (5)$$

where $\bar{u}$ is the horizontal wind at the center of each range gate, $u' = \frac{\partial u}{\partial z}\left(\frac{\Delta z}{2}\right)$ where $\frac{\partial u}{\partial z}$ is the wind shear and Δz is the gate spacing (105 m), θ is equal to 4.5°, the half-beam width of the profiler vertical beam, and w' is the maximum variation in vertical velocity associated with turbulence, which is assumed to be equal to u'. Solving for w, we obtain

$$w = \frac{V - \left(\bar{u} + u'\right)\sin\theta}{\cos\theta} - V_{T_{\min}} - w' . \qquad (6)$$

Equation (6) reduces to Eq. (3) in Battan (1973) for the case of an infinitely small beam width in which the horizontal wind has no effect on w.

The uncertainty in the estimation of w is given by

$$\Delta w = \sqrt{\underset{I}{\left(\Delta V \sec\theta\right)^2} + \underset{II}{\left(V \sec\theta \tan\theta \Delta\theta\right)^2} + \underset{III}{\left(\Delta\bar{u}\tan\theta\right)^2} + \underset{IV}{\left(\bar{u}\sec^2\theta\Delta\theta\right)^2} + \underset{V}{\left(\Delta u'\tan\theta\right)^2} + \underset{VI}{\left(u'\sec^2\theta\Delta\theta\right)^2} + \underset{VII}{\left(\Delta V_{T_{\min}}\right)^2} + \underset{VIII}{\left(\Delta w'\right)^2}} . \qquad (7)$$

The root-mean-square (rms) estimate of the uncertainties ΔV, $\Delta\bar{u}$, $\Delta u'$, $\Delta V_{T_{\min}}$, $\Delta w'$, and $\Delta\theta$ were determined in the following manner. The variable, $\bar{u}$, was determined from spatial and temporal interpolation of the wind speed (u) from soundings, assuming linearity. At worst, $\bar{u}$ could have had the value u of any of the soundings bounding the interpolation. The uncertainty, $\Delta\bar{u}$, was therefore determined by considering the rms difference between the interpolated value of $\bar{u}$ and each of the measured u from all the soundings used in the interpolation. The uncertainty $\Delta u'$ was determined in a similar way, except considering the sounding values of wind shear within the distance of a range gate. The uncertainty $\Delta w'$ was assumed to equal $\Delta u'$. The uncertainty ΔV was assumed to be the half-width of a spectral bin, 0.14 m s^{-1}. The uncertainty $\Delta V_{T_{\min}}$ based on the calculation of the terminal velocity of the smallest detectable particles was estimated to be 0.1 m s^{-1}. The uncertainty $\Delta\theta$ was assumed to be 1 degree. These uncertainties were determined for each individual band, since the sounding winds were different in each cyclone. Table 1 summarizes the values of the variables involved in the calculation of the uncertainty in vertical motion (Eq. 7), and Δw for each of the nine bands, each cyclone, and the complete analyzed data set. The uncertainty Δw ranged from 0.4 m s^{-1} to 0.8 m s^{-1}, with the overall Δw for the entire data set equal to 0.6 m s^{-1}.

3. OVERVIEW OF THE STORMS

The following sections provide an upper level thermodynamic overview and a composite radar depiction from three different winter storms that

Table 1. Uncertainties (m s^{-1}) in estimation of w

From Eq. 7:		*I*	*II*	*III*	*IV*	*V*	*VI*	*VII*	*VIII*	Δw
IOP1		0.14	0.00	0.46	0.22	0.02	0.00	0.10	0.24	0.6
	Band A	0.14	0.00	0.51	0.13	0.01	0.00	0.10	0.18	0.6
	Band B	0.14	0.00	0.43	0.21	0.02	0.00	0.10	0.23	0.6
	Band C	0.14	0.00	0.47	0.27	0.02	0.00	0.10	0.27	0.6
IOP2		0.14	0.00	0.57	0.36	0.01	0.00	0.10	0.15	0.7
	Band D	0.14	0.00	0.63	0.36	0.01	0.00	0.10	0.15	0.8
	Band E	0.14	0.00	0.63	0.36	0.01	0.00	0.10	0.15	0.8
	Band F	0.14	0.00	0.47	0.36	0.01	0.00	0.10	0.15	0.6
IOP3		0.14	0.00	0.44	0.18	0.02	0.00	0.10	0.23	0.6
	Band G	0.14	0.00	0.26	0.13	0.01	0.00	0.10	0.15	0.4
	Band H	0.14	0.00	0.48	0.20	0.03	0.00	0.10	0.32	0.6
	Band I	0.14	0.00	0.46	0.19	0.02	0.00	0.10	0.21	0.6
Overall		0.14	0.00	0.50	0.26	0.02	0.00	0.10	0.20	0.6

occurred in January and February 2004. The first storm took place in Flora, Illinois (southeastern Illinois) between 1200 UTC and 2300 UTC 25 January 2004 (IOP1). This storm was associated with a cyclone that developed east of the Rocky Mountains and tracked eastward across the central and southeastern United States. The latter two storms developed near the coast of the Gulf of Mexico and moved northeastward over the southeastern United States. The MIPS was deployed in Huntsville, Alabama (northern Alabama) during these two intensive operation periods, which took place from 0000 UTC 15 February to 0000 UTC 16 February 2004 (IOP2) and from 1600 UTC 25 February to 1200 UTC 26 February 2004 (IOP3).

A regional composite radar image for each IOP at the time of each event centered over the MIPS location is shown in Fig. 2. Figure 3 shows the signal-to-noise ratio (SNR) from the profiler in the left column and mean radial velocity $\overline{V_r}$ in the right column. SNR is the ratio of the returned signal power to the system noise power. The noise is approximately constant over an operational period, so variations in SNR when precipitation is present are closely related to variations in precipitation intensity. The minimum radial velocities were consistently below the melting layer during each IOP and represented faster-falling precipitation in the form of rain or freezing rain.

3.1 *IOP1, 25 January 2004, Southern Illinois*

The cyclone formed over Colorado around 0000 UTC 25 January 2004 and progressed southeastward into Oklahoma and Arkansas by 1200 UTC 25 January. The area sampled by the profiler was along a warm frontal boundary that extended from Missouri through South Carolina at 1200 UTC and moved north of the Ohio River Valley by 0000 UTC. A region of high relative humidity (greater than 70%) was present along the warm front, which was coincident with the region of precipitation illustrated on the radar composite (Fig. 2a).

The SNR profile during the precipitation event (1300 to 2200 UTC) revealed fine-scale bands that extended from the ground, vertically to as high as six kilometers (Fig. 3a). The bands ranged from approximately 5 to 35 km wide, were oriented roughly west to east, and moved northward at approximately 12 m s^{-1}. The surface precipitation alternated between freezing rain/drizzle mixed rain and ice pellets. Approximately 3 mm (one-eighth inch) of ice and 25 mm (one inch) of sleet had accumulated during the nine-hour period of precipitation at the profiler site in Flora, IL.

A sounding was launched from Lincoln, IL (KILX) at 1800 UTC 25 January (not shown) during the passage of the bands over Lincoln (about 180 km northwest of the profiler), representative of the profiled bands. The sounding showed an inversion up to 800 hPa with a stable, saturated atmosphere through 450 hPa, the approximate top of the bands appearing in Fig. 3a.

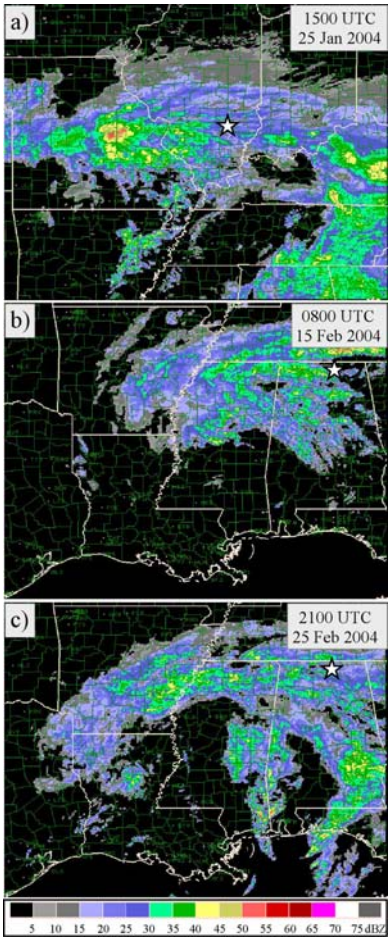

Figure 2. Composite base reflectivity for each IOP. On each panel, the star depicts the profiler location.

3.2 IOP2, 15 February 2004, Northern Alabama

The IOP2 cyclone was associated with a weak surface low over Mississippi at 0000 UTC 15 February 2004. A region of high relative humidity at 700 hPa extended from Georgia westward into Arkansas and was associated with a tongue of warm air, a feature termed the trough of warm air aloft, or trowal (see Martin 1998). The trowal progressively sharpened during the period that the bands passed over the profiler (0300 UTC to 1700 UTC 15 February, Fig. 3c) in Huntsville, AL.

Soundings show that at KBMX, a stable layer was present to the 850-hPa level, with a moist-adiabatic profile above that level. AT KBNA, the atmosphere was dry and stable to the 750-hPa level. Above that level the temperature profile was moist-adiabatic.

The precipitation started at the MIPS site in Huntsville, AL at about 0300 UTC in the form of rain. The bands between 0600 and 1200 UTC were 20 – 50 km wide and extended up to 6 km (Figs. 2b and 3c). The precipitation changed to mixed rain, snow and drizzle near 1200 UTC and continued as mixed precipitation until it ended at 1800 UTC.

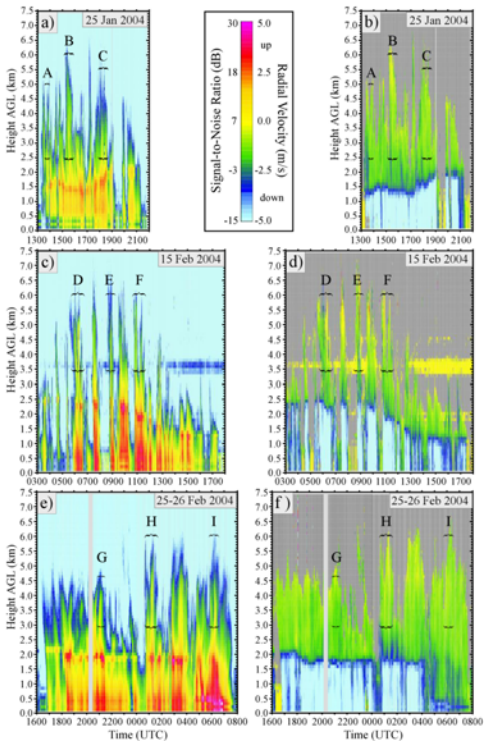

Figure 3. Time series of profiler signal-to-noise ratio (left panels) and radial velocity (right panels) for each IOP. Key is shown in upper center of figure. Negative values of radial velocity indicate motion toward profiler (downward). Lettered brackets correspond to the bands analyzed within each cyclone.

3.3 IOP3, 25-26 February 2004, Northern Alabama

At 1200 UTC 25 February 2004, a weak surface low pressure system was located over the Gulf of Mexico, south of Alabama and a band of moisture at 700 hPa stretched along and over this frontal boundary (not shown).

By 2100 UTC 25 February, a narrow region of precipitation extended in an arc from northeast Texas, northeastward to northern Alabama, and then southeastward into Georgia along this moisture axis (Fig. 2c). A second area of precipitation extended along the Alabama-Mississippi border. Both of these areas of precipitation passed over the profiler during the event. The area of precipitation along the arc reached the profiler location in Huntsville, AL around 1700 UTC 25 February. Several narrow bands (10-35 km in width) produced rain as they passed over the profiler. The bands were 4 – 4.5 km deep between 1700 UTC 25 February and 0000 UTC 26 February (Fig. 3e). The mean orientation of the bands was from west to east as they moved north-northeastward (Fig. 2c).

By 0000 UTC 26 February, the surface low had just moved onshore over southern Alabama and a trowal at 700 hPa was present from southeastern Arkansas through western Georgia. The KBMX sounding for 0000 UTC 26 February showed a stable layer present between 900 and 750 hPa, with a moist adiabatic temperature profile above that level to 450 hPa (the approximate top of the bands). Saturated air was present from 950 to 850 hPa and from 700 to 550 hPa, with dry air above.

Around 0100 UTC 26 February, the bands changed characteristics in that they increased to 6 km in height and were approximately 30 – 60 km wide. Shortly after 0400 UTC 26 February, the height of the melting level fell abruptly to just under 0.5 km (Figs. 3.4e,f). The precipitation changed from rain to a mixture of rain and wet snow until the precipitation ended after 0800 UTC.

4. VERTICAL MOTIONS WITHIN THE BANDS

Our goal was to determine the magnitudes of the vertical air motion within winter precipitation bands. It was impossible to estimate the terminal fall velocities once particles had started undergoing significant aggregation and melting as they approached the melting layer. Therefore, the calculations herein are limited to the layer extending from approximately one kilometer above the melting level to the top of each band for each IOP. In each case, we were interested in the vertical air motions at higher altitudes because the structure of the individual bands was most apparent at these altitudes (Fig. 3). The vertical air motions were deduced within the upper part of three bands in each IOP (Bands A-I in Fig. 3). The bands were chosen to represent a reasonable sample of all the bands within each IOP.

The vertical velocity (w) within Bands A-C of IOP1 is contoured in Figs. 4a-c. The portion of the bands where w was determined is outlined and overlaid on the SNR fields (Figs. 4d-f). Figures 5 and 6 are arranged similarly, except they show Bands D-F in IOP2 and Bands G-I in IOP3, respectively. All heights in these and subsequent profiler figures are above ground level (AGL).

Statistics for each band, each IOP and the overall study are summarized in Table 2. The table shows the number of w values used in the calculations, the minimum and maximum w values $\pm\Delta w$ from Table 1, the mean positive and negative values of w and the corresponding standard deviations, and the mean and standard deviation of w. The correlation coefficient between the SNR and w is also presented.

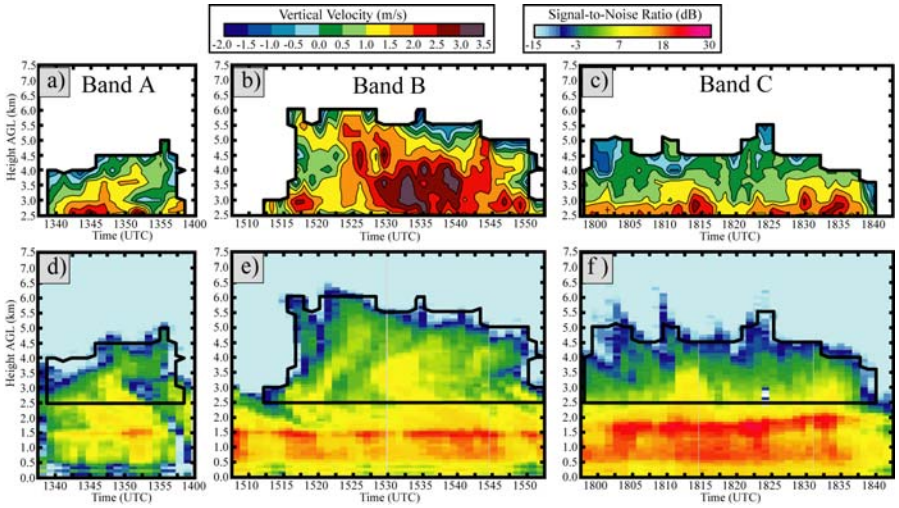

Figure 4. Derived vertical motion, w, (top panels) and signal-to-noise ratio (bottom panels) for three bands in IOP1 on 25 January 2004. Heavy boxes in bottom panels show the areas of each bands where w was determined.

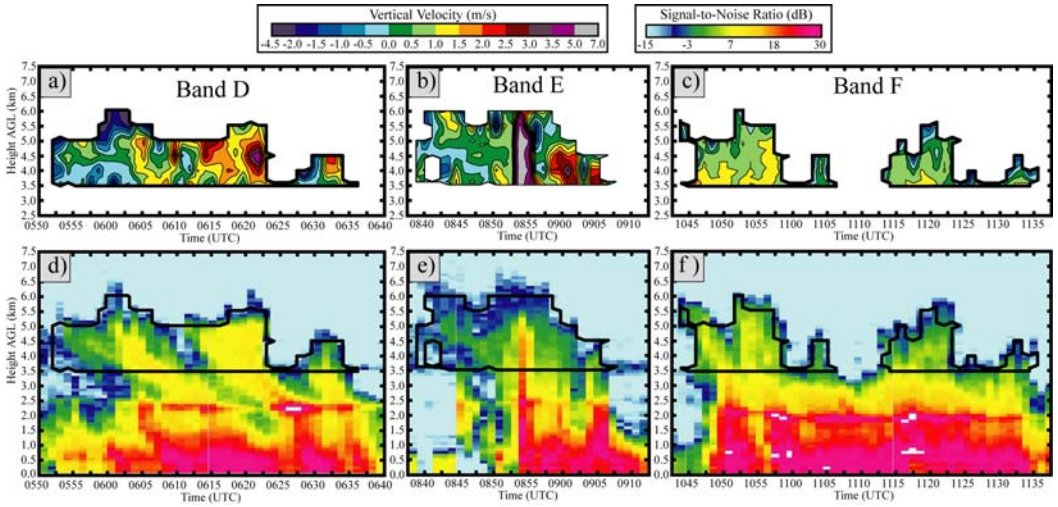

Figure 5. Same as Fig. 4 except for three bands in IOP2 on 15 February 2004.

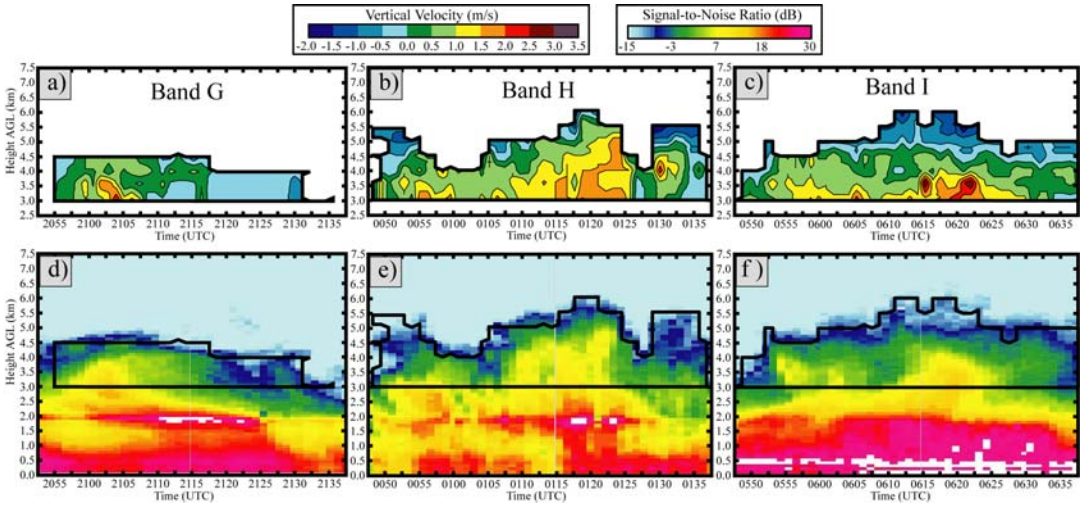

Figure 6. Same as Fig. 4 except for three bands in IOP3 on 25- 26 February 2004.

Table 2. Average values of w (m s^{-1}) and SNR-w correlation coefficient for each band, each IOP and all bands.

	A	B	C	D	E	F	G	H	I	IOP1	IOP2	IOP3	All
# of w values	83	234	197	159	127	135	125	219	236	514	421	580	1515
Min. w	-1.4	-2.2	-1.9	-4.3	-2.5	-2.3	-1.0	-2.1	-1.9	-2.2	-4.3	-2.1	-4.3
Max. w	3.3	3.6	2.9	4.3	6.7	1.9	2.7	2.4	3.0	3.6	6.7	3.0	6.7
Δw	0.6	0.6	0.6	0.8	0.8	0.6	0.4	0.6	0.6	0.6	0.7	0.6	0.6
Mean Pos. w	1.2	1.6	1.0	1.2	1.5	0.8	0.6	0.9	0.8	1.3	1.1	0.9	1.1
σ Mean Pos. w	0.6	0.8	0.7	0.8	1.6	0.4	0.5	0.5	0.5	0.8	1.1	0.5	0.9
Mean Neg. w	-0.5	-1.0	-0.8	-1.1	-0.7	-1.0	-0.3	-0.7	-0.7	-0.8	-1.0	-0.6	-0.7
σ Mean Neg. w	0.3	0.5	0.4	1.0	0.7	0.6	0.2	0.5	0.4	0.5	0.8	0.4	0.6
Mean w	0.7	1.3	0.7	0.4	0.8	0.3	0.1	0.5	0.3	1.0	0.5	0.3	0.6
σ Mean w	1.0	1.2	0.9	1.4	1.7	0.9	0.6	0.9	0.9	1.1	1.4	0.8	1.1
Corr. Coeff., r	0.85	0.76	0.85	0.60	0.66	0.71	0.68	0.72	0.85	0.79	0.59	0.76	0.68

5. SUMMARY

The goal of this study was to determine the magnitude of the vertical air velocities within precipitation bands in three winter cyclones. The cyclones occurred during January and February 2004 over the Midwestern and southern United States. The vertical air velocities were obtained from Doppler spectra measured by the vertical beam of the 915 MHz profiler mounted on the University of Alabama-Huntsville's Mobile Integrated Profiling System using the Lower Bound Method, which in this paper was adapted to account for spectral broadening due the mean horizontal wind, vertical wind shear, and turbulence. Vertical velocities were only derived between ~1 km above the melting level and the top of the bands. Within this layer, the fall velocities of the smallest detectable particles could be reliably estimated.

Derived vertical air motions ranged from -4.3 to 6.7 m s^{-1} with an uncertainty of about ±0.6 m s^{-1}. The upward motion within the bands averaged +1.1 m sec^{-1} with a standard deviation (σ) of 0.9 m s^{-1}, and the mean downward motion was -0.7 m s^{-1} with a standard deviation of 0.6 m s^{-1}. The average vertical motion found in the overall analysis was 0.6 m s^{-1} (σ = 1.1 m s^{-1}). Cumulative frequency diagrams showed that approximately 9% of the 1515 total observations of w had updrafts greater than 2.0 m s^{-1}, 35% exceeded 1.0 m s^{-1}, and 29% consisted of downward vertical motion. These values are generally consistent with previous studies in Pacific Northwest, except that more extreme values were observed in one band than have been previously reported.

There was a high correlation (r) between values of SNR and w within each band (r between 0.60 and 0.85), each IOP (r between 0.59 and 0.79) and the overall analysis (r of 0.68). The strongest updrafts were typically between 2.0 and 4.0 m s^{-1} and located near the center of each band, from approximately 1 km above the melting level to near the top. These updrafts were usually found within regions of high SNR (5 to 15 dB). Regions of downdrafts within the bands had maximum values between -1.0 and -4.3 m s^{-1} and were typically located along the edges of the bands in regions of low SNR (-5 to -15 dB). These results are consistent with snow growth and sublimation processes. As air ascends in an updraft the ice crystals grow, creating a stronger signal back to the profiler resulting in a higher SNR. Sublimation and cooling occurs along the edges of the bands, producing sinking air, and low values of SNR.

It was beyond the scope of this paper to determine the dynamical mechanism(s) forcing the bands in these three cyclones. We note, however, that the magnitudes of the vertical velocities in the core of the bands were comparable to theoretical predictions for moist symmetric instability, but only under an assumption of an inviscid atmosphere (Emanuel 1983). Since tubes of air ascending slantwise in a sheared environment are likely to be disrupted by turbulent mixing (Emanuel 1983, p. 2372), it would appear that the retrieved vertical velocities are somewhat larger than expected for moist symmetric instability. This suggests that other

instabilities, such as potential instability, may have contributed to the band development in these storms.

REFERENCES

Atlas, D., 1964: Advances in radar meteorology. *Advances in Geophysics*, **10**, Academic Press, 318-478.

——, R. C. Srivastava, and R. S. Sekhon, 1973: Doppler radar characteristics of precipitation at vertical incidence. *Rev. Geophys. Space Phys.*, **11**, 1-35.

Battan, L. J., 1973: Turbulence spreading of Doppler spectrum. *J. Appl. Meteor.*, **12**, 822-824.

——, and J. B. Theiss, 1966: Observations of vertical motions and particle sizes in a thunderstorm. *J. Atmos. Sci.*, **23**, 78-87.

Bennetts, D. A., and B. J. Hoskins, 1979: Conditional symmetric instability—A possible explanation for frontal rainbands. *Quart. J. Roy. Meteor. Soc.*, **105**, 945-962.

Bluestein, H. B., 1993: *Synoptic-Dynamic Meteorology in Midlatitudes.* Vol. 2, *Observations and Theory of Weather Systems.* Oxford University Press, 594 pp.

Donaldson, R. J., Jr., and R. Wexler, 1969: Flight hazards in thunderstorms determined by Doppler velocity variance. *J. Appl. Meteor.*, **8**, 128-133.

Emanuel, K. A., 1983: The Lagrangian parcel dynamics of moist symmetric stability. *J. Atmos. Sci.*, **40**, 2368-2376.

Foote, G. B., and P. S. du Toit, 1969: Terminal velocity of raindrops aloft. *J. Appl. Meteor.*, **8**, 249-253.

Geerts, B., and P. V. Hobbs, 1991: Organization and structure of clouds and precipitation on the mid-Atlantic coast of the United States. Part IV: Retrieval of the thermodynamic and cloud microphysical structures of a frontal Rainband from Doppler data. *J. Atmos. Sci.*, **48**, 1287-1305.

Hertzman O., and P. V. Hobbs, 1988: The mesoscale and microscale structure and organization of clouds and precipitation in midlatitude cyclones. Part XIV: Three dimensional airflow and vorticity budget of rainbands in a warm occlusion. *J. Atmos. Sci.*, **45**, 893-914.

——, ——, and J. D. Locatelli, 1988: The mesoscale and microscale structure and organization of clouds and precipitation in midlatitude cyclones. Part XVI: Three dimensional airflow and vertical vorticity budget for a warm front. *J. Atmos. Sci.*, **45**, 3650-3666.

Herzegh P. H., and P. V. Hobbs, 1980: The mesoscale and microscale structure and organization of clouds and precipitation in midlatitude cyclones. II: Warm frontal clouds. *J. Atmos. Sci.*, **37**, 597-611.

——, and ——, 1981: IV: Vertical air motions and microphysical structures of prefrontal surge clouds and cold frontal clouds. *J. Atmos. Sci.*, **38**, 1771-1784.

Hobbs, P. V., T. J. Matejka, P. H. Herzegh, J. D. Locatelli, and R. A. Houze, Jr., 1980: The mesoscale and microscale structure and organization of clouds and precipitation in midlatitude cyclones. I: A case study of a cold front. *J. Atmos. Sci.*, **37**, 568-596.

Houze, R. A., Jr., S. A. Rutledge, T. J. Matejka, and P. V. Hobbs, 1981: The mesoscale and microscale structure and organization of clouds and precipitation in midlatitude cyclones. III: Air motions and precipitation growth in a warm frontal Rainband. *J. Atmos. Sci.*, **38**, 639-649.

Innocentini, V., and E. dos Santos Caetano Neto, 1992: A numerical study of the role of humidity in the updraft driven by moist slantwise convection. *J. Atmos. Sci.,* **49,** 1092–1106

Knight D. J., and P. V. Hobbs, 1988: The mesoscale and microscale structure and organization of clouds and precipitation in midlatitude cyclones. Part XV: A numerical modeling study of frontogenesis and cold frontal rainbands. *J. Atmos. Sci.*, **45**, 915-930.

Locatelli, J. D., and P. V. Hobbs, 1974: Fallspeeds and masses of solid precipitation particles. *J. Geophys. Res.*, **79**, 2185-2198.

——, and ——, 1987: The mesoscale and microscale structure and organization of clouds and precipitation in midlatitude cyclones. Part XIII: Structure of a warm front. *J. Atmos. Sci.*, **44**, 2290-2309.

Martin, J. E., 1998: The structure and evolution of a continental winter cyclone. Part II: Frontal forcing of an extreme snow event. *Mon. Wea. Rev.*, **126**, 329-348.

Novak, D. R., L. F. Bosart, and D. Keyser, and J. S. Waldstreicher 2004: An observational study of cold season–banded precipitation in the northeast U.S. cyclones. *Wea. Forecasting*, **19**, 993-1010.

Passarelli, R. E., Jr., 1978: Theoretical and observational study of snow-size spectra and snowflake aggregation efficiencies. *J. Atmos. Sci.*, **35**, 882-889.

Persson, P. O. G., and T. T. Warner, 1995: The nonlinear evolution of idealized, unforced, conditional symmetric instability: A numerical study. *J. Atmos. Sci.,* **52,** 3449–3474.

Probert-Jones, J. R., and W. G. Harper, 1961: Vertical air motions in showers as revealed by Doppler radar. Proc., *Ninth Wea. Radar Conf.*, Boston, MA, Amer. Meteor. Soc., 225-232.

Rauber, R. M., M. K. Ramamurthy, and A. Tokay, 1994: Synoptic and mesoscale structure of a severe freezing rain event: The St. Valentine's Day ice storm. *Wea. Forecasting*, **9**, 183-208.

Rogers, R. R., S. G. Leblanc, S. A. Cohn, W. L. Ecklund, D. A. Carter, and J. S. Wilson, 1996: Profiler measurements of turbulence and wind shear in a snowstorm. *Beitr. Phys. Atmos.*, **69**, 27-36.

Sanders, F., and L. F. Bosart, 1985a: Mesoscale structure in the Megalopolitan snowstorm of 11-12 February 1983. Part I: Frontogenetical forcing and symmetric instability. *J. Atmos. Sci.*, **42**, 1050-1061.

——, and ——, 1985b, Mesoscale structure in the Megalopolitan snowstorm of 11-12 February 1983.

Part II: Doppler radar study of the New England snowband. *J. Atmos. Sci.*, **42**, 1398-1407.

Sienkiewicz, J. M., J. D. Locatelli, P. V. Hobbs, and B. Geerts, 1989: Organization and structure of clouds and precipitation on the mid-Atlantic coast of the United States. Part II: The mesoscale and microscale structures of some frontal rainbands. *J. Atmos. Sci.*, **46**, 1349-1364.

Wang P-Y., and P. V. Hobbs, 1983: The mesoscale and microscale structure and organization of clouds and precipitation in midlatitude cyclones. Part X: Wavelike rainbands in an occlusion. *J. Atmos. Sci.*, **40**, 1950-1964.

——, D. B. Parsons, and P. V. Hobbs, 1983: The mesoscale and microscale structure and organization of clouds and precipitation in midlatitude cyclones. Part VI: Wavelike rainbands associated with a cold frontal zone. *J. Atmos. Sci.*, **40**, 543-558.

Wolfsberg, D. G., K. A. Emanuel, and R. E. Passarelli, 1986: Band formation in a New England winter storm. *Mon. Wea. Rev.*, **114**, 1552-1569.

Xu, Q., 1992: Formation and evolution of frontal rainbands and geostrophic potential vorticity anomalies. *J. Atmos. Sci.*, **49**, 630-648.

Zhang, D.-L., and H.-R. Cho, 1995: Three-dimensional simulation of frontal rainbands and conditional symmetric instability in the Eady-wave model. *Tellus,* **47A**, 45-61.